Check for updates

Received: 10 May 2022 | Revised: 25 August 2022 | Accepted: 29 August 2022

DOI: 10.1111/boc.202200038

Biology of the Cell

RESEARCH ARTICLE

The distal central pair segment is structurally specialised and contributes to IFT turnaround and assembly of the tip capping structures in *Chlamydomonas* flagella

Ambra Pratelli | **Dalia Corbo** | **Pietro Lupetti** | **Caterina Mencarelli**

Department of Life Sciences, University of Siena, Siena, Italy

Correspondence
Caterina Mencarelli, Department of Life Sciences, University of Siena, Via Aldo Moro 2, 53100 Siena, Italy.
Email: caterina.mencarelli@unisi.it

Abstract

Background Information: Cilia and flagella are dynamic organelles whose assembly and maintenance depend on an activetrafficking process known as the IntraFlagellar Transport (IFT), during which trains of IFT protein particles are moved by specific motors and carry flagellar precursors and turnover products along the axoneme. IFT consists of an anterograde (from base to tip) and a retrograde (from tip to base) phase. During IFT turnaround at the flagellar tip, anterograde trains release their cargoes and remodel to form the retrograde trains. Thus, turnaround is crucial for correct IFT. However, current knowledge of its mechanisms is limited.

Results: We show here that in Chlamydomonas flagella the distal ~200 nm central pair (CP) segment is structurally differentiated for the presence of a ladder-like structure (LLS). During IFT turnaround, the IFT172 subunit dissociates from the IFT- B protein complex and binds to the LLS-containing CP segment, while the IFT-B complex participates in the assembly of the CP capping structures. The IFT scaffolding function played by the LLS-containing CP segment relies on anchoring components other than the CP microtubules, since IFT turnaround occurs also in the CP-devoid pf18 mutant flagella.

Conclusions: During IFT turnaround in Chlamydomonas flagella, i) the LLS and the CP terminal plates act as anchoring platforms for IFT172 and the IFT-B complex, respectively, and ii) during its remodeling, the IFT-B complex contributes to the assembly of the CP capping structures.

Significance: Our results indicate that in full length Chlamydomonas flagella IFT remodeling occurs by a specialized mechanism that involves flagellar tip structures and is distinct from the previously proposed model in which the capability to reverse motility would be intrinsic of IFT train and independent by any other flagellar structure.

KEYWORDS
IntraFlagellar Transport (IFT), cilia, flagellar tip, immunolabelling, electron tomography

Abbreviations: IFT, Intraflagellar transport; CP, Central pair; TAP, Tris Acetate Phosphate; HEPES, 2-[4-(2-hydroxyethyl)piperazin-1-yl]ethanesulfonic acid; NP-40, Nonidet P-40; PBS, Phosphate-buffered saline; BSA, Bovine Serum Albumine; LSS, Ladder-like structure.

This is an open access article under the terms of the Creative Commons Attribution License, which permits use, distribution and reproduction in any medium, provided the original work is properly cited.
© 2022 The Authors. *Biology of the Cell* published by Wiley-VCH GmbH on behalf of Société Française des Microscopies and Société de Biologie Cellulaire de France.

1768322x, 2022, 12, Downloaded from https://onlinelibrary.wiley.com/doi/10.1111/boc.202200038 by University Of Siena Sist Bibliot Di Ateneo, Wiley Online Library on [21/12/2022]. See the Terms and Conditions (https://onlinelibrary.wiley.com/terms-and-conditions) on Wiley Online Library for rules of use; OA articles are governed by the applicable Creative Commons License

INTRODUCTION

Cilia and flagella are thin appendages extending from the surface of most eukaryotic cells where they play crucial motility and/or sensory functions. In humans, ciliary defects result in a number of genetic diseases collectively indicated as ciliopathies (Braun & Hildebrandt, 2017; Reiter & Leroux, 2017). To perform their functions, these organelles evolved a highly specialised structural organisation, based on a central microtubular core – the axoneme – formed by a ring of nine doublet microtubules that extend from the cell-anchoring basal body up to the distal tip district, where their assembly takes place (Johnson & Rosenbaum, 1992; Rosenbaum & Child, 1967). Such a microtubule arrangement occurs mostly in sensory cilia, and is commonly referred to as 9+0. On the contrary, most motile axonemes exhibit a 9+2 pattern, which is characterised by the additional presence of the central pair (CP) apparatus, consisting of two singlet microtubules and their associated projections.

For most of its length, the CP maintains a uniform ultrastructural organisation, which has been accurately established by cryo-electron tomographic analyses (Carbajal-González et al., 2013; Teves et al., 2016), and is involved in the regulation of axonemal motility. In the distal segment, on the contrary, the B-tubules of axonemal doublets end, the CP loses all its projections, and peculiar capping structures occur at the plus end of the remaining microtubules (Dentler, 1980; Ringo, 1967) . These structures are still poorly characterised. Very little information is in fact available on the ultrastructural and molecular organisation of the ciliary tip. This region has been visualised by negative staining of demembranated cells in the two protist species, *Tetrahymena termophila* and *Chlamydomonas reinhardtii*. In these organisms, thin distal filaments emerge from a plug inserted into the lumen of each A-tubule, and the CP is capped by a complex structure consisting of transversal plates lying over the tubule ends with an overhead 'bead', or ring (Dentler & Rosenbaum, 1977; Dentler, 1980). No information on the molecular composition of the cap and the distal filaments is currently available, mainly for the extreme liability of these components that has hampered their isolation and biochemical analysis. Less ultrastructurally defined tip components have been reported to occur in other types of cilia (Croft et al., 2018; Soares et al., 2019).

Once assembled, cilia and flagella are dynamic organelles, subjected to a continuous turnover (Marshall & Rosenbaum, 2001). Both ciliary assembly and maintenance depend on IntraFlagellar Transport (IFT), which allows flagellar precursors to reach the assembly site at the ciliary tip, and turnover products to be carried back to the cell body (Nakayama & Katoh, 2020; Taschner & Lorentzen, 2016). Most of the main molecular actors implicated in IFT have been identified. They include two motors, the anterograde kinesin-2 (Kozminski et al., 1995) and the retrograde dynein-2 (Pazour et al., 1999; Porter et al., 1999), along with two protein complexes, named IFT-A and IFT-B, comprising 6 and 16 subunits, respectively (Taschner & Lorentzen, 2016). The IFT-A and IFT-B complexes interact with each other to form linear polymers, the IFT trains, which act as platforms for cargoes and are moved by the two motors in the space between the microtubule doublet surface and the membrane. Anterograde and retrograde trains have different architectures and distinct structural features, the latter displaying a looser structure with a typical zig-zag profile, and the former showing an electron-dense, compact appearance (Jordan et al., 2018). Hence, a significant remodelling must occur once the trains reach the flagellar tip for the anterograde train to discharge its cargoes, reorganise into the retrograde train to take on turnover products, and transit from a kinesin-2 to a dynein-2 mediated movement. Nevertheless, the conversion from one transport phase to the other, commonly known as the turnaround process, is still one of the less defined steps of the whole IFT process. In *Chlamydomonas*, kinesin-2 moves back to the ciliary base by diffusion (Chien et al., 2017). Multiple evidence demonstrated that IFT trains shuttle continuously between the ciliary tip and base, without significant pauses (Dentler, 2005; Engel et al., 2009). Some kinases have been implicated in the detachment of kinesin-2 from anterograde IFT trains in different organisms (Chaya et al., 2014; Ichinose et al., 2015; Liang et al., 2014; Oh et al., 2019). However, to date the available data are far from depicting a complete pathway for IFT remodelling at the ciliary tip.

In order to provide further insights into the morpho-functional organisation of the ciliary tip, we decided to undertake electron microscopy, immunolocalisation and electron tomographic analyses on the distal district of *Chlamydomonas* flagella. Our results provide an in-deeper definition of a structural component that is specific of the terminal CP segment, and has been previously known as the tip sheet (Ringo, 1967). In addition, we provide evidence that the IFT-B complex is directly involved in the assembly and is part of the capping structures located at the CP end.

MATERIALS AND METHODS

Strains and culture conditions

C. reinhardtii strains used in the work include wild-type strain 137cc mt^+ and the mutant strains CC-5159(*ift74-1*), CC-1919 (*fla10-1*^{ts}), CC-1920 (*fla11*^{ts}) and CC-1036 (*pf18*). They were all grown in Tris Acetate Phosphate (TAP) buffer (Gorman & Levine, 1965) at 22°C, on a light-dark cycle of 14–10 h, under a constant 5% CO_2 aeration, except the strain CC-5159 that was grown

1768322x, 2022, 12, Downloaded from https://onlinelibrary.wiley.com/doi/10.1111/boc.202200038 by University Of Siena Sist Bibliot Di Ateneo, Wiley Online Library on [21/12/2022]. See the Terms and Conditions (https://onlinelibrary.wiley.com/terms-and-conditions) on Wiley Online Library for rules of use; OA articles are governed by the applicable Creative Commons License

overnight without aeration as described in Brown et al. (2015).

Negative staining and immunolabelling

Chlamydomonas cells suspended in 10 mM HEPES, pH 7.4, were left to adhere onto polylysine-treated 300-mesh Formvar carbon-coated grids. Grids were then transferred upside-down for 30 s onto a droplet of 0.1% NP-40 in HM buffer (10 mM Hepes, pH 7.4, 2 mM Mg^{2+}); after several washes in HM and in H_2O_{dd}, grids were negatively stained with 2% uranyl acetate in aqueous solution. To observe flagellar tips after inhibition of Ca^{2+}-dependent protein kinases, grid-absorbed cells were transferred for 30 s onto a droplet of HM containing either W7(A3281, Sigma-Aldrich) or the 1294 compound (kindly provided by Dr. Wesley Van Voorhis, Department of Medicine, University of Washington), at a concentration of 5 μM, and successively demembranated and negatively stained as described above.

For immunolabelling, after detergent treatment grids were washed in HM, fixed in 0.2% glutaraldehyde, 4% paraformaldehyde (IEM grade) in HM, washed again in HM, transferred in phosphate-buffered saline (PBS), pH 7.4, and sequentially incubated for 30 min in 0.1 M glycine in PBS, and for 30 min in 0.1% BSA in PBS. Grids were then incubated for 2 h onto a droplet of the antibody solution, at a dilution of 1:1. Primary antibodies included three mouse monoclonals specific for the IFT139, the IFT172, or the IFT81 subunit, and a rabbit polyclonal antibody raised to the IFT74 subunit. Antibodies were kindly donated by Prof. Joel Rosenbaum, Yale University (USA).

After washing in PBS, grids were incubated for 2 h with the gold-conjugated secondary antibody (10 nm gold-conjugated anti-mouse IgG, Sigma G7527, or 10 nm gold-conjugated anti- rabbit IgG, Sigma G7402), used at a dilution of 1:20. Finally, grids were sequentially washed in PBS and in H_2O_{dd}, then negatively stained as described above.

Transmission electron microscopy

Cells were processed for flat-embedding in Epon resin according to Geimer (2009). Flat-embedded cells were cut with a Reichert Ultracut IIE ultramicrotome equipped with a Diatome Ultra 45° diamond knife. Thin sections (60 nm) were collected on formvar-coated 75- or 100-square mesh copper grids and stained with uranyl acetate and lead citrate (Reynolds, 1963). Samples were imaged by a FEI Tecnai G2 Spirit transmission electron microscope operating at an electron-accelerating voltage of 100 kV and fitted with an OSIS Morada CCD camera and ITEM software.

Electron tomography and 3D modelling

Thick sections (≈280–300 nm) from flat-embedded flagella of wild-type cells were decorated on both faces with 10-nm colloidal gold particles before TEM analysis. Gold particles were used as fiducial markers for image alignment during the tomogram reconstruction procedure. Tomography was performed with a Philips CM200 transmission electron microscope fitted with a field emission gun and a CCD TVIPS F224HD camera. Series of tomographic images were recorded at an electron accelerating voltage of 200 kV and at 27,500× magnification using TVIPS EMMenu and EMTool softwares. For tomographic reconstruction, series of tilted images were recorded at low electron dose, in double-tilt axis geometry, with a maximum tilt range of about 60° and tilt steps of 1°. After the first series was recorded, the grid was extracted by the microscope, rotated by 90° and a second tilt series was recorded along the orthogonal tilting axis. IMOD software (http://bio3d.colorado.edu/imod/index.html) was used for image stakes alignment and tomograms assembly (Kremer et al., 1996). The signal-to-noise ratio was increased with mad_eed_3d application (Frangakis & Hegerl, 2001) from IMOD software. The obtained models underwent manual segmentation arbitrarily assigning different colours to each detectable component at flagellar tip, using UCSF Chimera (Pettersen et al., 2004).

Statistical analysis of IFT172 gold labelling distribution in wild-type versus *fla11^{ts}* mutant cells

Count data (i.e., the number of gold particles observed per CP) were imported in R (ver. 3.4.4; R core team, 2021). Normality of the data was tested using the Shapiro–Wilk normality test and equal variance using the F test in r-base. The existence of overall differences in the number of gold particles across conditions was tested using the Kruskal–Wallis rank sum test and pairwise differences among conditions using a post hoc Wilcoxon rank sum test with Benjamini–Hochberg correction for multiple comparisons.

RESULTS

The terminal segment of the CP complex is ultrastructurally differentiated from the axonemal shaft

In *Chlamydomonas*, the architecture of the flagellar terminal segment – ~0.2 μm long – is distinct from that of the axonemal shaft. The boundary between the two regions can be detected by the abrupt interruption of

1768322x, 2022, 12, Downloaded from https://onlinelibrary.wiley.com/doi/10.1111/boc.202200038 by University Of Siena Sist Bibliot Di Ateneo, Wiley Online Library on [21/12/2022]. See the Terms and Conditions (https://onlinelibrary.wiley.com/terms-and-conditions) on Wiley Online Library for rules of use; OA articles are governed by the applicable Creative Commons License

the radial spokes sequence and the clearer appearance of the flagellar matrix (Figure 1a, arrow). In the terminal region the diameter of the flagellum progressively decreases for the ending, first, of the B-tubules and, more distally, of the A-tubules, while the CP persists almost to the very end of the flagellum to form the pointed tip that is typical of full-length flagella. The CP terminates in a transversal plate, beyond which a clear and approximately conical space is visible, which hosts the CP capping structures (Figure 1a,b). The latter are not directly evident in sections of embedded specimens, but can be observed in demembranated, negatively stained flagella (Figure 2a,b).

Besides the cap, the terminal CP segment is distinguished by a peculiar structural component, that is, a stripe of electron-dense material intercalated between the two microtubules (Figure 1b, white bracket). In transversal sections of flagella, such intertubular material is absent along the axonemal shaft (Figure 1d) while in the terminal segment it appears as a barrel-like element with enlarged ends (Figure 1e,f). This component has been previously indicated as the tip sheet (Lechtreck et al., 2013; Ringo, 1967), and is currently very poorly characterised.

After negative staining of demembranated flagella, the terminal CP segment exhibits, besides the two tubules and the capping structures, a series of transversal stripes that appear either to be intercalated between the two tubules or to extend laterally (Figure 2a,b), depending on the way the CP lies on the grid. Such a series of stripes had been interpreted by Dentler (1980) as an helicoidal filament wrapping the tubules (Figure 1c).

In order to gain insight into the structural organisation of the tip sheet, we exposed grid-absorbed, detergent-treated flagella to low temperature (4°C, 1 h). Such a treatment results in the solubilisation of the CP tubules, and allows to visualise a residual ladder-like structure, which we will mention hereinafter as the LLS, consisting of a central amorphous axis with thin lateral projections that emerge from both of its sides and terminate with small globular regions (Figure 2c–g). We note that after cold treatment the LLS is still continuous with the cap and is linked by thin connections to the terminal plate (arrowheads in Figure 2d–g). The latter is not continuous but rather is divided into two separated parts. The LLS projections are grouped in modules, each one consisting of four projections. Within each module, the first projection is separated from the second one by 10.7 ± 0.4 nm, the second from the third one by 16.3 ± 1.3 nm, and the third from the fourth by 16.3 ± 1.3 nm (dots in Figure 2c). The number of modules observed in each LLS may vary from 1 to 3 with an interspace of about 24.2 ± 1.9 nm between adjacent modules. We observed LLSs with variable lengths, up to 200 nm. Thus, the LLS appear to possess quite a strict geometry. As reported by Lechtreck et al. (2013), this component is not present in the earlier phase of flagellar assembly, but appears only

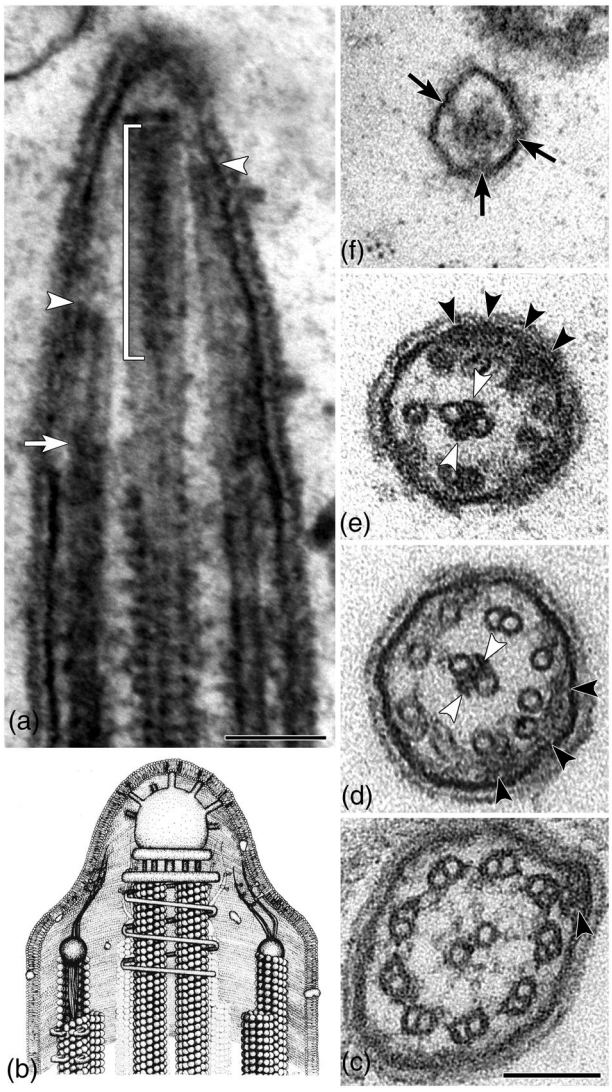

FIGURE 1 TEM analysis of the distal CP segment in *Chlamydomonas* flagella. In the longitudinal sections shown in (a), the white arrow marks the ultrastructural transition from the CP shaft, characterised by the occurrence of repeating radial spokes, and the distal CP segment. Arrowheads point to the termination of A tubules. The tip sheet is encompassed by the squared bracket, and the apparently empty space located between the CP end and the membrane comprises the capping structures (terminal plates and the ring) which are poorly visible in sections from embedded samples. As a reference, the original schematic of the tip architecture proposed by Dentler (1980) is reported in (b). The cross sections shown in (c–f) are cut at different distances from the flagellar tip and show the architectural modifications that occur along the flagellar length, from the doublet region (c), up to the distal tip-sheet region, where the B-tubules, first, and then the A-tubules progressively decrease in number (d and e), and disappear at the very distal tip (f). In (d–e), white arrowheads indicate the electron-dense tip sheet intercalated between the two microtubules of the CP, and black arrowheads indicate electron-dense IFT trains. In F, the compact ends of the CP tubules are visible, presumably corresponding to the terminal plates; the electron-dense material that is still associated with the membrane is connected to the CP by bridges (black arrows). Bar = 100 nm.

1768322x, 2022, 12, Downloaded from https://onlinelibrary.wiley.com/doi/10.1111/boc.202200038 by University Of Siena Sist Bibliot Di Ateneo, Wiley Online Library on [21/12/2022]. See the Terms and Conditions (https://onlinelibrary.wiley.com/terms-and-conditions) on Wiley Online Library for rules of use; OA articles are governed by the applicable Creative Commons License

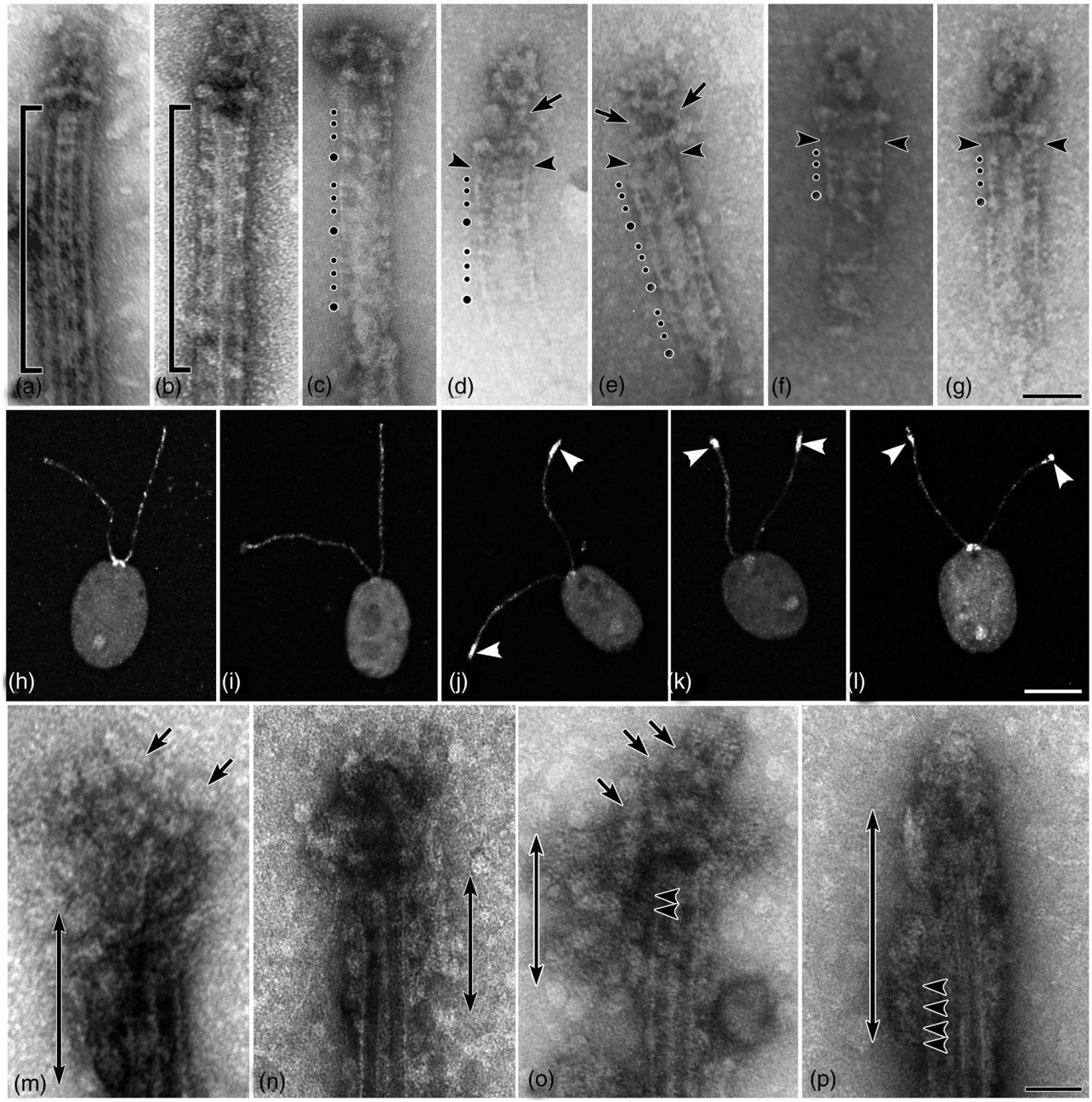

FIGURE 2 Upper panel: analysis of the tip sheet, or ladder-like structure (LLS), after negative staining of demembranated, unextracted (a and b) or cold-extracted (4°C, 1 h) (c–g) flagella. The LLS appears as a series of transversal lines in the region indicated by brackets in (a and b), a morphology previously interpreted as an helicoidal filament wrapping the distal CP region (see Figure 1c). The periodicity typical of this axonemal component is indicated by dots in (c–g). Note that the LLS maintains a close connection with the capping structures also after cold treatment. Arrowheads indicate the thin filaments connecting the LLS to the terminal plates, the arrows indicate the connections between the ring and the terminal plates. Bar = 50 nm.

Middle panel: Analysis of the effect exerted by CDPK-1 inhibition on IFT distribution along the flagellum. Cells expressing IFT20-mCherry protein were observed before (h and i) and after 30 s exposure (j and k) to the 1294 inhibitor or to the W7 inhibitor (l). Arrowheads indicate the IFT20 accumulation at the flagellar tip, suggestive of a defective turnaround. Bar = 5μm. Lower panel: visualisation of IFT particles accumulated around the distal CP end after exposure of cells to CDPK-1 inhibitors (1294, m–n, or W7, o–p), followed by membrane removal and negative staining (m–p). Both globular particles and thin elongated elements are present, some of which are indicated, respectively, by arrows and arrowheads. Double arrows indicate regions of particle binding along the CP tubules, where binding appears to be mediated by thin elongated particles. Bar = 50 nm.

1768322x, 2022, 12, Downloaded from https://onlinelibrary.wiley.com/doi/10.1111/boc.202200038 by University Of Siena Sist Bibliot Di Ateneo, Wiley Online Library on [21/12/2022]. See the Terms and Conditions (https://onlinelibrary.wiley.com/terms-and-conditions) on Wiley Online Library for rules of use; OA articles are governed by the applicable Creative Commons License

after 20 min regeneration, being thus typical of flagella longer than half length.

The LLS-containing region is involved in IFT turnaround

In our negatively stained samples of demembranated flagella, we occasionally observed particulate material inserting between the microtubule ends and the cap. Since the morphology of this material after negative staining is reminiscent of that of isolated IFT particles (Mencarelli et al., 2013), we hypothesised that the terminal CP segment and its cap might be involved in IFT turnaround. In *Chlamydomonas*, the currently available information indicates that this process initiates at the ciliary tip with the release of kinesin-2 from the IFT-B complex, an event that is consequent to the phosphorylation of the kinesin FLA8 subunit by CDPK-1, a Ca^{2+}-dependent kinase (Liang et al., 2014). Hence, inhibition of this kinase is expected to block the turnaround path. We reasoned that, if the CP is indeed involved in IFT turnaround, then inhibitors of Ca^{2+}- dependent kinases would increase the amount of IFT components associated with the CP.

We used two kinase inhibitors - W7, a general inhibitor for Ca^{2+}-dependent kinases, and 1294, a synthetic inhibitor specific for apicomplexan CDPK-1 (Castellanos-Gonzalez et al., 2013). Both compounds, when tested on cells expressing IFT20-mCherry, induce the accumulation of IFT20 at the flagellar tip (Figure 2, middle panel). This phenotype is typical of cells unable to undergo IFT turnaround. When cells were exposed to any one of the two inhibitors before membrane removal and negative staining, the CP end was found to be surrounded by piles of IFT-like particles, consisting of both roundish and thin, elongated particles (Figure 2, lower panel), similar, respectively, to the IFT-A and IFT-B complex (Jordan et al., 2018). The latters were often observed to interact laterally also with the surface of the terminal CP segment.

These observations indicate that Ca^{2+}-dependent kinase inhibitors negatively interfere with IFT turnaround. The accumulation of IFT particles around the distal CP segment and the direct insertion of IFT-B-like particles on the distal CP microtubular surface suggest that this region of the CP might be directly involved in the anterograde to retrograde IFT transition.

IFT defects or disruption lead to the disappearance of the ring component of the cap

To further check the relationship occurring between the CP terminal segment and IFT, we decided to analyse

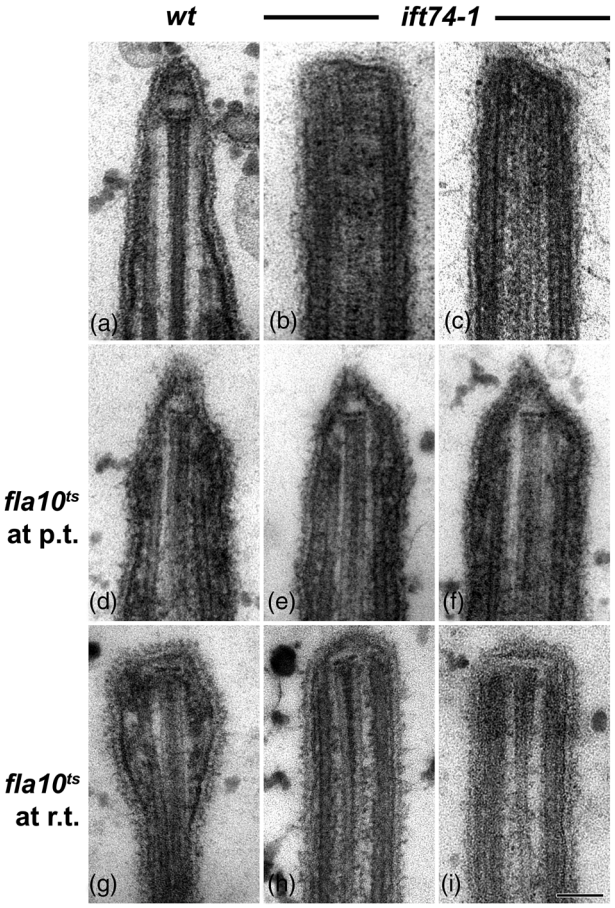

FIGURE 3 Comparative TEM imaging of the tip phenotype in wild-type flagella (a) and in two mutant strains defective in IFT turnaround, the *Chlamydomonas ift74-1* strain (b–c) and the *fla10-1^{ts}* strain. *ift74-1* flagella possess a flat tip, while *fla10-1^{ts}* flagella show a phenotype similar to the wild-type phenotype at the permissive temperature (p.t. = 22°C, d–f), and a flat tip phenotype after 1 h at the restrictive temperature (r.t. = 32°C (g–i)). Bar = 100 nm.

two *Chlamydomonas* mutants with defective IFT, the *ift74-1* strain, expressing a truncated IFT74 protein that lacks the N-terminal 196 residues (Brown et al., 2015), and the temperature-sensitive *fla10-1^{ts}* strain, carrying a point mutation at residue 329 of the FLA10 motor domain (Kozminski et al., 1995) (Figure 3).

The *ift74-1* mutant strain assembles only half-length flagella (Brown et al., 2015). We found that *ift74-1* flagella do not exhibit the cone-shaped tip typical of wild-type flagella and are instead characterised by a flat end (Figure 3a–c). The CP is as long as the doublets, and the membrane is closely lining the axoneme end, a feature that is indicative of the absence of any capping structure.

In the *fla10-1^{ts}* mutant, IFT undergoes a complete cycle at the permissive temperature of 22°C, but is interrupted at the restrictive temperature of 32°C due to the inactivation of kinesin-2 and the subsequent block of anterograde transport. Interestingly, we found that

1768322x, 2022, 12, Downloaded from https://onlinelibrary.wiley.com/doi/10.1111/boc.202200038 by University Of Siena Sist Bibliot Di Ateneo, Wiley Online Library on [21/12/2022]. See the Terms and Conditions (https://onlinelibrary.wiley.com/terms-and-conditions) on Wiley Online Library for rules of use; OA articles are governed by the applicable Creative Commons License

fla10-1^{ts} flagella exhibit distinct phenotypes at the permissive and restrictive temperature. At the permissive temperature of 22°C, *fla10-1*^{ts} flagella exhibit the typically pointed tip of wild-type flagella (fig.3D-F). On the contrary, after incubation of cells at the restrictive temperature (32°C) for 1 h, when IFT cycling is interrupted and flagellar resorption is just beginning, *fla10-1*^{ts} flagella display instead a flat phenotype, indicative of the absence of the cap (Figure 3g–i).

These findings indicate that the presence of the cap structures is related to and depends on the occurrence of an active IFT cycle.

The LLS and the cap are associated structures that assemble even in the absence of the CP

In order to verify if the concomitant presence of the CP tubules is a mandatory requisite for the assembly of both the LLS and the cap, we analysed the *Chlamydomonas pf18* mutant strain. These cells are unable to assemble the CP complex, which is replaced by an amorphous central core (Adams et al., 1981).

Surprisingly, LLSs assembled in an ectopic position could be observed also in *pf18* flagella, either associated with the end of one of the A tubules or centrally located (stripes in Figure 4a–d). Following membrane removal, pf18 microtubule doublets keep their 9+0 bundle arrangement and do not split from each other (unshown data), thus impairing visualisation of any component located in the central core of the axoneme. After cold treatment (4°C for 1 h), however, doublets partially separate, sometimes revealing the occurrence of an LLS-like component with an associated cap (Figures 4e and S1). Ring-like structures could be sometimes observed even without cold treatment at the end of an A-tubule after negative staining of demembranated flagella (arrows in Figure 4f). These rings could be immunolabelled by an anti-IFT74 antibody (Figure 4g).

These findings suggest that the LLS and the cap are associated structural components even in the absence of the CP tubules, and that the ring may interact with IFT proteins.

Distinct IFT-B components differentially interact with the distal CP district

Hence, IFT trains might be endowed with an intrinsic capability to reverse their motility. This simpler mechanism of anterograde-to-retrograde conversion might underlie the first rapid phase of flagellar assembly, being more compatible with the large amounts of IFT particles that encompass the growing flagellar tip during early regeneration. In Chlamydomonas (and possibly also in other organisms) IFT-B anchoring to the LLS-containing region of the CP and the subsequent formation of the cap might be part of a more specialised mechanism of turnaround that is acquired later during flagellar elongation and characterises full-length flagella. In order to confirm that IFT components actually interact with the CP, we performed a series of immunoelectron microscopy (IEM) using IFT antibodies on grid-absorbed, demembranated cells. These experiments were carried out in the absence of kinase inhibitors to allow a clearer visualisation of the capping structures. Since IFT trains dissociate and are recovered in the soluble matrix/membrane fraction after membrane removal (Cole et al., 1998; Piperno & Mead, 1997), any labelling observed under these experimental conditions is expected to target only those IFT components that remain associated with the distal CP complex after detergent treatment.

We used antibodies for the IFT139 subunit of the IFT-A complex and for the IFT74, IFT81 and IFT172 subunits of the IFT-B complex.

Despite of several immunolocalisation experiments, we have never been able to observe any labelling using the IFT139 antibody on demembranated flagella. This finding suggested that IFT-A might be solubilised along with the membrane by the detergent treatment. On the contrary, all IFT-B antibodies reacted positively with demembranated flagella and marked the distal CP segment.

Interestingly, labelling with the IFT172, IFT74 and IFT81 antibodies showed distinct spatial distributions.

IFT172 revealed a localisation along the CP that is strictly confined to the LLS-containing segment (Figure 5). Gold particles were not found more distally than or at the terminal plates. On the contrary, IFT74 and IFT81 antibodies were found to label mainly the cap structures (terminal plates and the ring) (Figure 6). The two antibodies show overlapping labelling distributions, in agreement with the fact that IFT74 and IFT81 proteins are involved in the formation of a heterodimer (Lucker et al., 2005).

The almost reciprocal labelling patterns we obtained with the IFT172 and IFT74/81 antibodies is evident in the drawing shown in Figure 7a, which summarises the positions on the distal CP segment of all the gold particles detected in our immunolocalisation experiments.

The whole set of immunoelectron microscopy experiments indicates that the IFT172, IFT74 and IFT81 subunits differentially interact with the CP, with the former interacting only with the LLS-containing CP region and the two latters being also localised on the ring, distally to the terminal plates. The strong IFT74/IFT81 labelling observed at this site suggests that the IFT-B complex might either interact with or be a main component of the cap.

1768322x, 2022, 12, Downloaded from https://onlinelibrary.wiley.com/doi/10.1111/boc.202200038 by University Of Siena Sist Bibliot Di Ateneo, Wiley Online Library on [21/12/2022]. See the Terms and Conditions (https://onlinelibrary.wiley.com/terms-and-conditions) on Wiley Online Library for rules of use; OA articles are governed by the applicable Creative Commons License

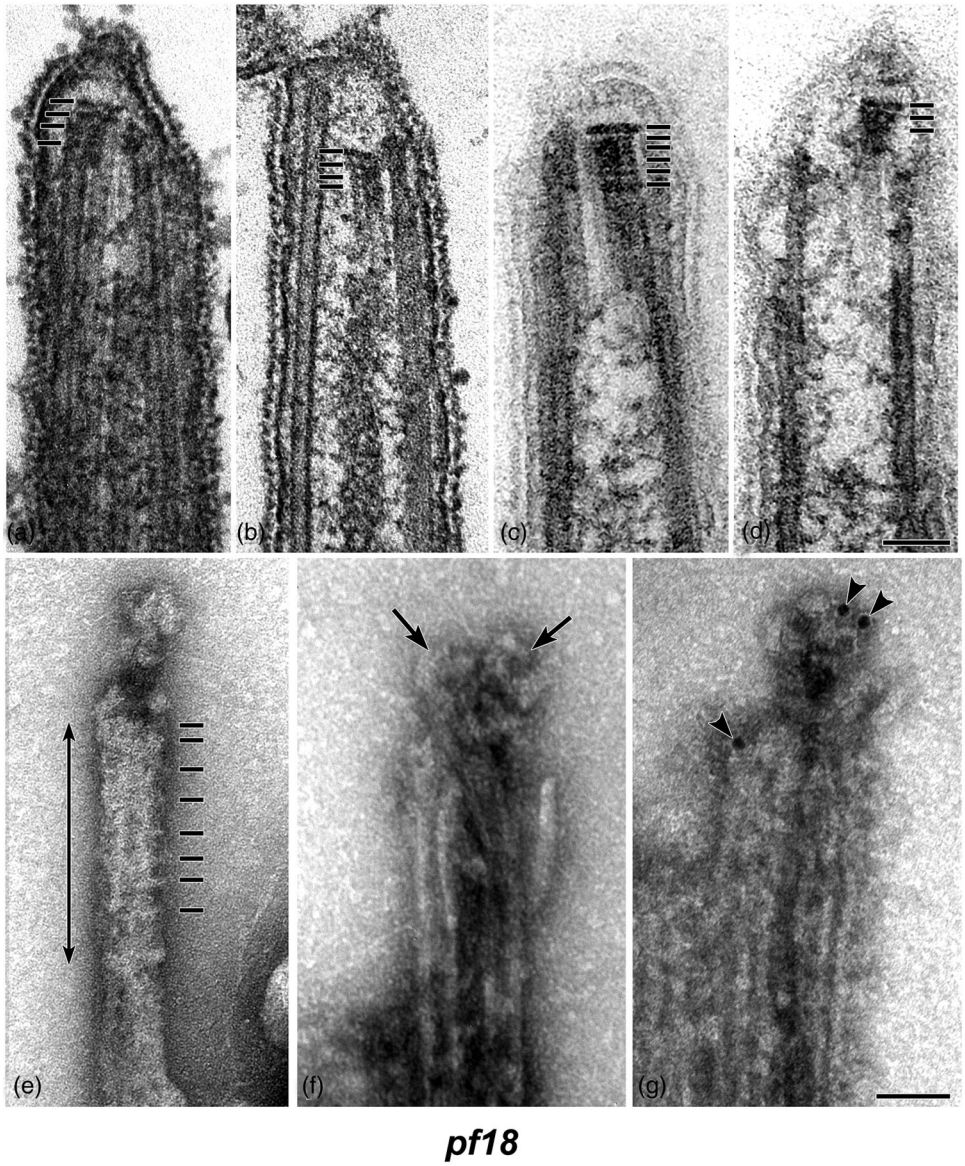

FIGURE 4 An ectopic LLS is visible in sections of resin-embedded *pf18* mutant flagella observed by TEM (stripes in (a–d)). After negative staining of cold-treated (4°C 1 h) demembranated flagella, *pf18* doublet bundles partially separate, revealing the occurrence of an LLS-like component associated with the distal part of A-tubules (stripes in (e)). The double arrow in (e) indicates the length of the LLS-like component. See also Figure 1S for the whole picture. Ring-like arrangements can also be found at the end of A tubules in demembranated *pf18* axonemes not subjected to cold treatment (arrows in (f)). After IFT74 immunolabelling of grid-absorbed, demembranated cells, such arrangements are decorated by gold particles (arrowheads in (g)). Bars = 100 nm.

The possibility that IFT172 might be involved in IFT turnaround had been previously indicated by the analysis of *fla11*^{ts}, a temperature sensitive mutant strain that carries a single-point mutation at residue 1615 of the protein (Pedersen et al., 2005). At the restrictive temperature (32°C), this mutant accumulates IFT proteins at the flagellar tip, a feature indicative of a defective turnaround. Using the same immunolocalisation protocol described above, we analysed IFT172 labelling in the *fla11*^{ts} mutant at both the permissive and the restrictive temperature and compared it with that observed in wild-type flagella. The number of gold particles per CP found in wild-type flagella at room temperature and in *fla11*^{ts} flagella at either the permissive or restrictive temperature is reported in Figure 7b. The Kruskas–Wallis test indicated significant differences ($p < 0.001$) in the number of gold particles/CP among the three samples. The post hoc test indicated significant differences too, although with different support (wild-type vs *fla11* p.t and *fla11* p.t. vs *fla11* r.t.: $p < 0.01$; wild-type vs. *fla11* r.t.: $p < 0.001$). Compared to wild-type, labelling intensity was slightly reduced in *fla11*^{ts} flagella at the permissive temperature, but was considerably reduced at the restrictive temperature.

1768322x, 2022, 12, Downloaded from https://onlinelibrary.wiley.com/doi/10.1111/boc.202200038 by University Of Siena Sist Bibliot Di Ateneo, Wiley Online Library on [21/12/2022]. See the Terms and Conditions (https://onlinelibrary.wiley.com/terms-and-conditions) on Wiley Online Library for rules of use; OA articles are governed by the applicable Creative Commons License

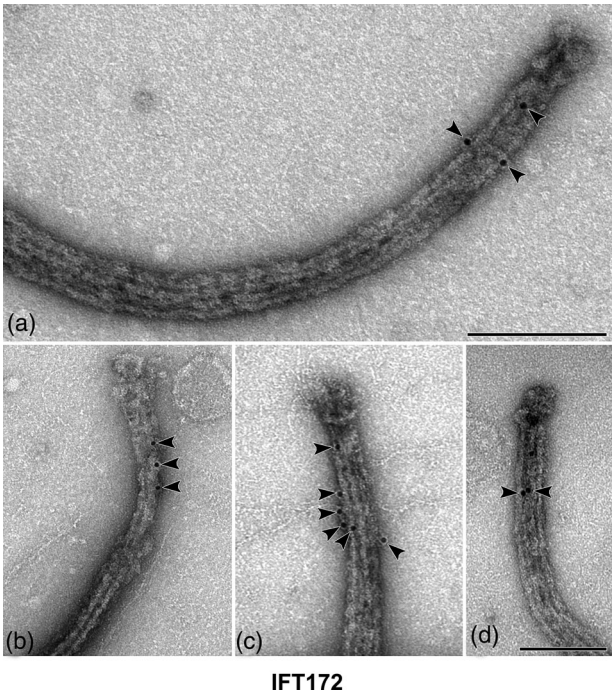

FIGURE 5 IFT172 immunolabelling is restricted to the LLS-containing distal ~200 nm CP segment. Grid-absorbed, demembranated cells were immunolabelled and successively negatively stained (see M&M for the whole procedure). Labelling is not found on the capping structures. Black arrowheads indicate the gold particles. Bars = 200 nm.

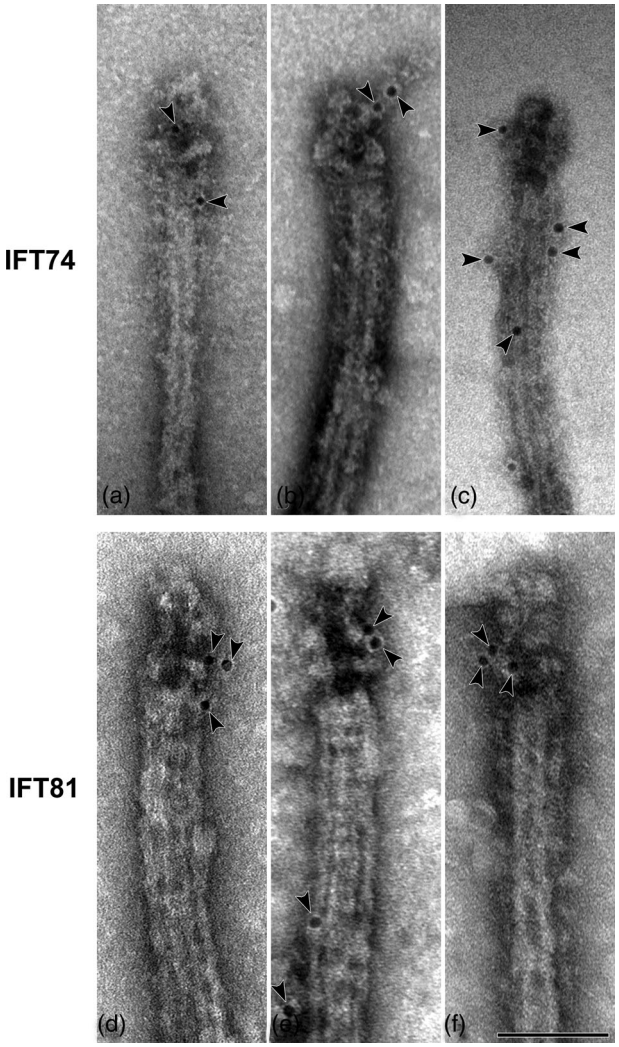

FIGURE 6 IFT74 (a-c) and IFT81 (d-f) immunolabelling of the distal ~200 nm CP segment. Grid-absorbed, demembranated cells were immunolabelled and successively negatively stained (see M&M for the whole procedure). Labelling was found to be more frequent on the capping structures than on the LLS-containing CP region. Black arrowheads indicate the gold particles. Bar = 100 nm.

Hence, *fla11*^{ts} mutant flagella exhibit a reduced binding of IFT172 to the LLS-containing region of the CP.

These observations provide a basis for the *fla11*^{ts} permissive and restrictive phenotypes described by Pedersen et al. (2005) and, as a whole, suggest that i) during IFT turnaround IFT172 dissociates from IFT-B and anchors to LLS, ii) that IFT-B may be a component of the ring.

Electron tomographic analysis of *Chlamydomonas* flagellar tip

The tip district has till now escaped any detailed analysis by 3D electron tomography, since its high complexity and structural variability make the subtomogram averaging, required for high-resolution 3D modelling, extremely difficult. To mitigate this problem, we decided to perform our tomographic analysis on single flat-embedded flagellar tips, avoiding averaging of subtomograms from different flagellar tip tomograms. Such an analytical strategy, though leading to a lower resolution, provided useful insights into the spatial 3D relationships existing between IFT trains and the CP capping structures in situ. The same approach has already been employed to compare growing and mature flagellar tips in *Chlamydomonas* and *Trypanosoma* (Höög et al., 2014).

In virtual longitudinal sections of double tilt axis tomograms from embedded flagella, IFT trains contacting the CP terminus can often be found distally to the end of the A-tubule. Here, the train seems to split into two components, with the inner part of the train contacting the CP terminal plates and the outer part remaining associated with the membrane (black arrowheads and black arrows, respectively, in Figure 8; see also Videos S1–S4). Such a feature was observed in 8 out of 22 tomograms we analysed. The 3D model shown in Figure 8d–h was obtained by manual segmentation of one of these tomograms, that was selected for the presence of two IFT trains in proximity of the tip (indicated in Figure 8a by brackets). The train on the left is ~50 nm wide (Figure 8c) and

1768322x, 2022, 12, Downloaded from https://onlinelibrary.wiley.com/doi/10.1111/boc.202200038 by University Of Siena Sist Bibliot Di Ateneo, Wiley Online Library on [21/12/2022]. See the Terms and Conditions (https://onlinelibrary.wiley.com/terms-and-conditions) on Wiley Online Library for rules of use; OA articles are governed by the applicable Creative Commons License

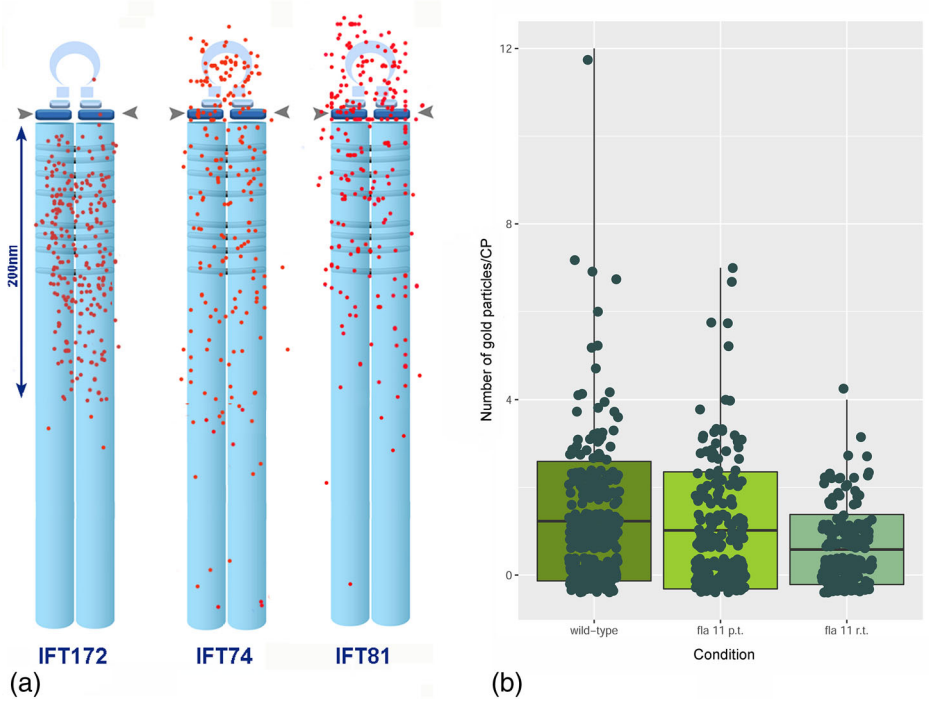

FIGURE 7 a) Schematic distribution of all the gold particles localised throughout all the immunolabelling experiments. For each antibody, the number of observed flagella and the total number of counted gold particles was, respectively, 142 and 243 (IFT172), 143 and 209 (IFT74), 159 and 224 (IFT81). (b) Distribution of gold particles/CP in wild-type and in *fla11*^{ts} flagella at different temperatures. Boxes indicate mean ± standard deviation, whiskers indicate range. The data are overplotted (jittered; n = 319, 211, 199, respectively), Figure 6b was created in ggplot2 (Wickham, 2016).

exhibits the compact organisation typical of the anterograde trains (Pigino et al., 2009; Stepanek & Pigino, 2016). The IFT train on the right shows instead a looser structure and the zig-zag pattern (the repeat of which is indicated in Figure 8a by dots) characteristic of the retrograde trains. The tomogram substack shown in Figure 8b suggests that both the anterograde and the retrograde train might establish a contact with the distal CP end.

Some considerations can be drawn from the 3D model shown in Figure 8d,e.

First, the anterograde train, shown in different pink shades, is confirmed to split at a level corresponding approximately to the end of the A-tubule (arrow in Figure 8d). The outer part (light pink) of the train remains bound to the membrane and merges with the dense material scattered onto the inner surface of the membrane at the very distal tip district. The innermost part (pink) moves closer to the CP and contacts its distal end, while a third, intermediate mass (in magenta) seems to stop before reaching the very distal flagellar tip. The terminal plate could not be identified in our segmentation map, likely due to the low map resolution.

Second, the most distal tip district, which is located beyond the termination of the CP tubules and is expected to contain the CP capping structures, appears to comprise multiple elongated elements (in violet) (Figure 8d), which are shown at a greater magnification and under different vantage points in Figure 2f–h. These are reciprocally arranged in a roughly parallel fashion (Figure 8h) and converge towards a central ring-like component (in red), that likely corresponds to the ring or 'bead' described by Dentler (1980).

Third, the ring-like component and the innermost part of the anterograde train contact the same restricted area just above the LLS distal end, from which also the retrograde train emerges.

The whole set of ultrastructural data indicate that the distal segment of the CP is specialised for function/s distinct from the axonemal shaft and suggests that it might play a direct role in the anterograde to retrograde IFT conversion.

DISCUSSION

The flagellar tip is a central district in ciliary function, being the site of both signalling events and IFT turnaround (Croft et al., 2018). In *Chlamydomonas*, it is characterised by the exclusive presence of two till now poorly studied components – the cap, located at the CP end, and the LLS, interposed between the two CP microtubules and formerly known as the tip sheet. The new information we provide here may contribute to elucidate the role that these components play in tip-

1768322x, 2022, 12, Downloaded from https://onlinelibrary.wiley.com/doi/10.1111/boc.202200038 by University Of Siena Sist Bibliot Di Ateneo, Wiley Online Library on [21/12/2022]. See the Terms and Conditions (https://onlinelibrary.wiley.com/terms-and-conditions) on Wiley Online Library for rules of use; OA articles are governed by the applicable Creative Commons License

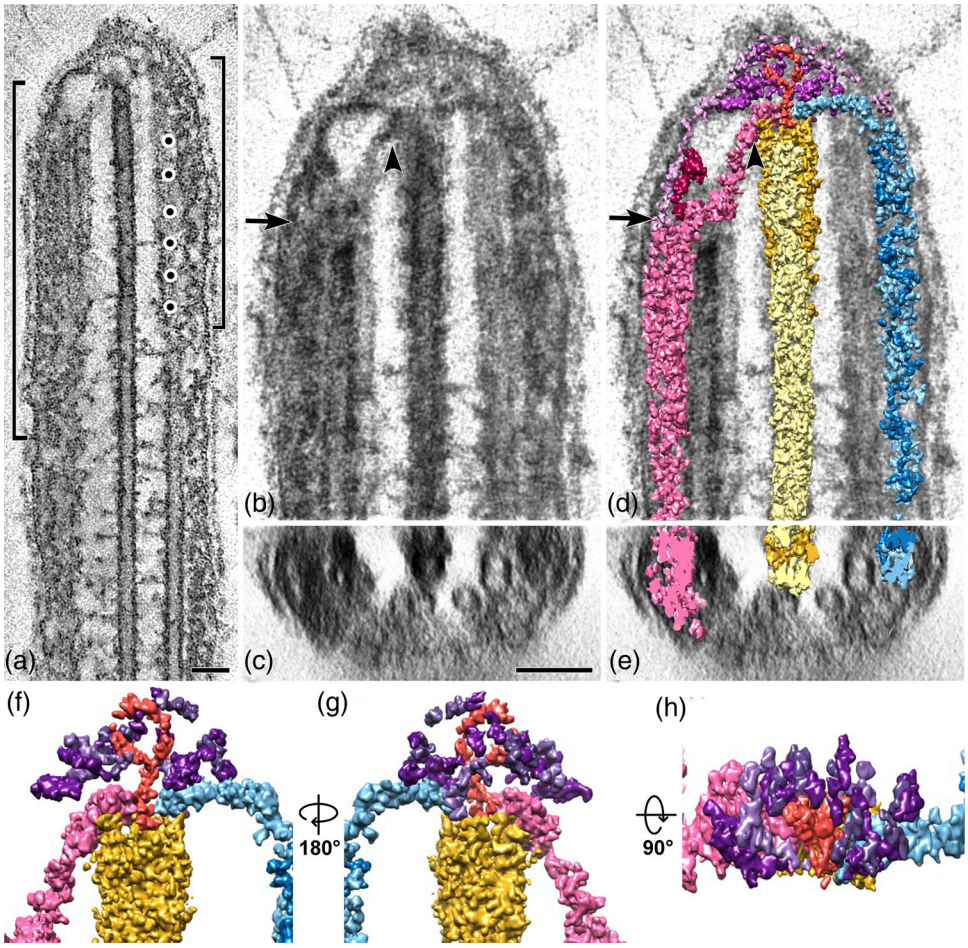

FIGURE 8 Electron tomographic analysis of the flagellar tip district. IFT trains (squared brackets in (a)) are visible as electron-dense material closely apposed to the flagellar membrane. The train on the right in (a,b) has the distinctive zig-zag pattern of the retrograde trains (dots in (a)). In (b–e) the tip region from the same tomogram is shown at a higher magnification in longitudinal (b,d) and in cross (c,e) sections, and is aligned in (d,e) with the regions of the segmentation 3D-model corresponding to i) the anterograde train (pink) and the three distal parts originated by train splitting after the termination of the A tubule (light pink, magenta, and pink), ii) the retrograde train (light blue and blue), iii) the ring (red) and the elongated short ribbons converging towards it (violet), iv) the CP tubules and the LLS (light yellow and gold yellow, respectively). Bars = 50 nm. The very distal components of the segmentation 3D-model are shown at a higher magnification and from different vantage points in (f–h). Both the innermost region of the anterograde train (pink) and retrograde train (light blue) converge onto the CP terminus, and a series of short ribbons (in violet) appears to be closely associated with the ring (red).

specific functions and, in particular, in the mechanism of anterograde-to-retrograde IFT conversion.

Our results show that the LLS is characterised by a peculiar and well-defined geometry, being composed of a central amorphous axis with thin projections extending from both sides and arranged in a repeating module. With respect to the helicoidal filament proposed by Dentler (1980) to enwrap the CP tubules we think that such a ladder-like geometry is more compatible with the different but strictly established distances we observed between successive pairs of lateral projections. In fact, in order to accomplish such a pattern, an helix should change its pass repeatedly. Notably, the central axis is continuous with the cap ring. Immunolocalisation data reveal that the LLS likely contains IFT-B proteins and that, in particular, it is likely to act as a scaffold for IFT172 anchoring. At this regard, it is interesting to note that the morphology and size of the LLS projections are similar to the 'open' conformation that this subunit may assume in vitro, consisting of a 30 nm-long rod-like region with a ~10 nm terminal globular domain (Wang et al., 2018). Whichever the function of the LLS, this is expected to be required only in flagella longer than half-length, since the assembly of the LLS-containing CP segment is delayed compared to the main CP region and occurs only at ~20 min regeneration time, when the flagellum is about 6 μm long (Lechtreck et al., 2013). The appearance of the LLS is concomitant with the formation of the capping structures. In fact, a recent electron tomographic study on regenerating *Chlamydomonas* flagella has confirmed that the capping structures form only after the phase of rapid flagellar elongation, that is, after the

1768322x, 2022, 12, Downloaded from https://onlinelibrary.wiley.com/doi/10.1111/boc.202200038 by University Of Siena Sist Bibliot Di Ateneo, Wiley Online Library on [21/12/2022]. See the Terms and Conditions (https://onlinelibrary.wiley.com/terms-and-conditions) on Wiley Online Library for rules of use; OA articles are governed by the applicable Creative Commons License

first 20–30 min of regeneration (Reynolds et al., 2018). As a consequence of the assembly of the cap, the tip acquires at that time the tapered conformation that is typical of the steady-state flagella. It is worth to note, at this regard, that flagellar half-length is a threshold length at which significant changes occur in the dynamics of IFT entry (Ludington et al., 2013; Vannuccini et al., 2016). Along with the finding that the LLS and the cap remain associated after cold extraction, their concomitant appearance during flagellar regeneration suggests that the two structures might be functionally related.

We show here that the cap is at least partially contributed by IFT-B proteins. No information has been previously reported on the molecular composition of the cap. Our conclusion is based on both immunolocalisation data and the tip morphology exhibited by two mutants with defective IFT, the strain *ift74-1* (Brown et al., 2015) and the strain *fla10-1^{ts}* when maintained at the restrictive temperature (Kozminski et al., 1995). In fact, in both strains the occurrence of a flat tip phenotype, indicative of the absence of any capping structures, is concomitant with the absence or the interruption of IFT cycling. Cells of the *ift74-1* strain express an N-terminally truncated IFT74 protein and assemble very short flagella (<4 μm) that are characterised by the presence of stalled IFT-B aggregates, a severely reduced IFT frequency and the inability to undergo retrograde transport. As a consequence, they do not carry on a cycling IFT process (Brown et al., 2015). In this mutant, assembly of short flagella is likely to be mainly based on diffusion, a process that contributes much more tubulin than IFT (Craft Van De Weghe et al., 2020). Concurrently, these mutant flagella have a flat tip, devoid of any capping structure. The same flagellar phenotype is exhibited by *fla10-1^{ts}* cells exposed at the restrictive temperature for 60 min. This strain expresses a FLA10 subunit with a point mutation in the motor domain and is unable to assemble a functional motor complex when cells are grown at 32°C; as a consequence, IFT can no longer proceed and stops completely within 60–90 min at the restrictive temperature (Kozminski et al., 1995). Concomitantly, the cap disassembles and the flagellar tip flattens. Thus, the cap is present only when a fully cycling IFT system is established, and an intact IFT-B complex, able to interact with the terminal CP surface, is expressed. Interestingly, a similar phenotype was also described for the *Roc22* mutant (Satish- Tammana et al., 2013). This is an insertional mutant null for FAP256/Cep104, a protein localised at the plus end of both the CP and the A tubules, that has been reported to interact with IFT74 (see fig. S2 in Al-Jassar et al., 2017). The IFT-B contribution to the assembly of the cap may account for its instability and, consequently, for the difficulties that have so far hampered its biochemical purification.

As a whole, immunolocalisation data and analysis of IFT-defective mutants suggest that both LLS and the cap might be involved in IFT turnaround. This is further sustained by our electron microscopy and electron tomographic analyses, both of which have shown that the innermost part of the IFT anterograde train, which is assembled by IFT-B (Jordan et al. 2018), bends inwards at the tip to contact the CP. In addition, incubation of cells with inhibitors of CDPK-1, a kinase that in *Chlamydomonas* is required to release kinesin-2 from IFT-B (Liang et al., 2014), results in the arrest of IFT turnaround and in the piling of IFT particles at the tip, both around the cap and along the terminal CP segment.

Which functional implications may our results have for the comprehension of IFT turnaround?

First, our data suggest not only that the cap is composed by IFT-B proteins but also that there is a correlation between the presence of the capping structures and the achievement of a fully cycling IFT. As a consequence, the turnaround mechanism as it occurs in the steady-state flagellum would be established only in flagella longer than about half-length. While steady-state flagella have smaller and frequent IFT injections, massive and infrequent injections occur early during regeneration to sustain the phase of rapid flagellar growth (Ludington et al., 2013). It seems thus plausible that, in short flagella, retrograde trains reorganise from the massively injected IFT material following a different and simpler mechanism that does not require the interaction with the CP and is independent from the presence of the cap. Indeed, the capability of IFT trains to reverse their direction at different points along the flagellum, before arriving at the tip, has been occasionally observed and has been recently experimentally induced (Nievergelt et al., 2022). Hence, IFT trains might be endowed with an intrinsic capability to reverse their motility. This simpler mechanism of anterograde-to-retrograde conversion might underlie the first rapid phase of flagellar assembly, being more compatible with the large amounts of IFT particles that encompass the growing flagellar tip during early regeneration. In *Chlamydomonas* (and possibly also in other organisms) IFT-B anchoring to the LLS-containing region of the CP and the subsequent formation of the cap might be part of a more specialised mechanism of turnaround that is acquired later during flagellar elongation and characterises full-length flagella. Under this point of view, it is interesting to note that *Chlamydomonas pf18* mutant flagella, which are almost as long as wild type flagella but are devoid of the CP tubules, still assemble in an ectopic position an LLS structure with an associated cap and are able to undergo at their tip a normal anterograde-to-retrograde conversion (Dentler et al., 2009). On the contrary, the short flagella assembled under stress (hypoxia) by the *ift74-1* strain and

1768322x, 2022, 12, Downloaded from https://onlinelibrary.wiley.com/doi/10.1111/boc.202200038 by University Of Siena Sist Bibliot Di Ateneo, Wiley Online Library on [21/12/2022]. See the Terms and Conditions (https://onlinelibrary.wiley.com/terms-and-conditions) on Wiley Online Library for rules of use; OA articles are governed by the applicable Creative Commons License

devoid of any capping structures only rarely show IFT traces in TIRF, and the rare IFT trains often reverse their direction before arriving at the tip (Brown et al., 2015).

The role played by the IFT172 subunit during IFT turnaround deserves a special attention. In fact, the distinct and complementary immunolocalisation patterns observed for IFT172 and the IFT74/IFT-81 subunits indicate that IFT-B turnaround requires the dissociation of IFT172 from the rest of the complex. In fact, only IFT74 and IFT81 labelling is found distally to the CP terminal plates, while IFT172 labelling is restricted to the LLS-containing segment and does not extend beyond the CP terminal plates. Alternatively, the absence of IFT172 labelling from the cap might be due to the epitope becoming inaccessible due to a protein conformational change occurring during IFT turnaround. However, we consider the latter possibility unlikely since, among all IFT-B proteins, IFT172 is endowed with a number of unique properties that fit well with its proposed dissociation behaviour at the flagellar tip.

First, IFT172 is characterised by a looser association with the IFT-B complex, from which it detaches at mild ionic conditions (Cole et al., 1998). Second, the expression of a defective IFT172 protein in both *Chlamydomonas* and *Tetrahymena* mutant strains results in the accumulation of IFT material at the ciliary tip, thus suggesting a possible role for this protein in IFT turnaround. In *Chlamydomonas*, analysis of the turnaround-defective *fla11*^{ts} strain, which carries a missense mutation in the C-terminal region of the protein, has revealed that a soluble IFT172 pool, not complexed with other IFT proteins, can bind to the plus-end microtubule binding protein EB1 (Pedersen et al., 2005). Accordingly, IFT172 is the only IFT protein containing the SxIP motif (residues 392SEIP395), known to identify proteins able to bind EB1 (Buey et al., 2012). In *Tetrahymena*, the expression of a partially truncated IFT172 protein lacking part of the evolutionarily conserved C-terminal alpha helix–rich repeat domain (RPD) is sufficient for anterograde IFT and ciliary assembly, but causes aberrant accumulation of the truncated protein itself and of other IFT components at the ciliary tip (Tsao & Gorovsky, 2008). Thus, in both species IFT turnaround is compromised when the C-terminal domain of the IFT172 protein is defective.

Our results show that the dissociated IFT172 subunit binds to the very last segment of the central complex, which is structurally specialised due to the presence of the LLS. The reduced efficiency of IFT172 binding we observed at the restrictive temperature in *fla11*^{ts} flagella indicates that the mutated form of the protein does not correctly interact with its binding site on the CP, and suggests that the C-terminal RPD region may provide a structural module required for IFT172 interaction with its ciliary tip anchoring component/s during IFT remodelling.

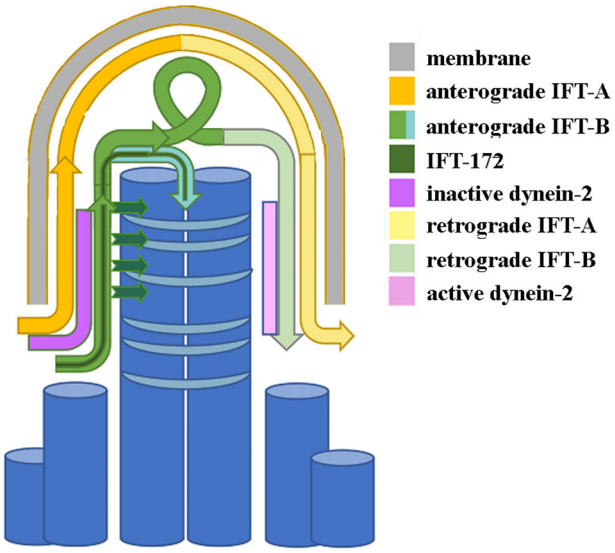

FIGURE 9 Schematic drawing of the hypothetical pathways followed by different IFT components during their turnaround at the flagellar tip, based on our results.

The dissociation of IFT172 from the IFT-B complex might occur during the interaction of the IFT-B complex with the terminal plates and/or through the lateral interaction with the distal CP surface. In this respect, we note that the variable LLS length, which is up to 200 nm long, corresponds to the CP segment that is not surrounded by the peripheral A-tubules, thus being exposed and freely accessible to protein interaction/s. IFT172 dissociation might be mediated by post-translational modification/s, given that this protein is predicted to have several ubiquitylation and phosphorylation sites (https://www.phosphosite.org/proteinAction.action?id=13383&showAllSites=true). Taken together, our data provide a tenable explanation for the turnaround defect observed in *fla11*^{ts}, and indicate that, during anterograde to retrograde conversion, IFT172 dissociates from IFT-B and anchors to the LLS-containing CP segment.

Our interpretation of our results is summarised in the provisional model for IFT turnaround shown in Figure 9. Close to the end of the A-tubule, the anterograde train splits, with the IFT-A complex remaining associated with the membrane and the IFT-B complex moving inward to contact the CP. The dissociation of IFT172 from IFT-B would be an early event of the turnaround process. After dissociation, this subunit would anchor to the LLS while the rest of IFT-B undergoes turnaround. During this phase, IFT-B anchoring to the CP terminal area could facilitate turnaround by preventing the complex from diffusing away. IFT-B would provide a backbone structure that, during turnaround, bends on itself forming ring-like structures and rearranges in order to assume the conformation required to assemble the retrograde

1768322x, 2022, 12, Downloaded from https://onlinelibrary.wiley.com/doi/10.1111/boc.202200038 by University Of Siena Sist Bibliot Di Ateneo, Wiley Online Library on [21/12/2022]. See the Terms and Conditions (https://onlinelibrary.wiley.com/terms-and-conditions) on Wiley Online Library for rules of use; OA articles are governed by the applicable Creative Commons License

train. Finally, the IFT-B backbone, coming off the CP terminal area in the proper configuration, would reassociate with IFT172, active dynein and IFT-A to assemble the retrograde train. In the proposed model, the LLS and the CP terminal plates act as anchoring platforms for IFT172 and the IFT-B, respectively. This possibility is in agreement with the pausing behaviour of IFT-B evidenced at the tip by in vivo studies on IFT dynamics carried out in *C. elegans, Trypanosoma*, and *Chlamydomonas*, which indeed suggests that IFT-B may be spatially restricted and anchored to some tip components (Buisson et al., 2013; Chien et al., 2017; Mijalkovic et al., 2017; Qin et al., 2007). In other ciliary models, some anchoring components, more elusive because less structurally specialised than the LLS, might play an equivalent function, being possibly associated with the A-tubules as we have observed in the *pf18* mutant. It is worth to note that the events we propose to occur during IFT turnaround at the flagellar tip follow a sequence that is reverse to that reported for IFT train assembly at the flagellar base, a process depending on IFT74 (Brown et al., 2015; Kanie et al., 2017; Nishijima et al., 2017).

The original model proposed by Pedersen et al. (2006) predicted a three-step process involving both the release of motors and the dissociation of IFT-A from IFT-B at the tip, which would hence be expected to contain soluble IFT components (the two IFT-A and IFT-B complexes, and the two motors kinesin-2 and dynein-2), which are instead bound to each other along the flagellar shaft, being assembled into anterograde and retrograde trains. Our results, on the contrary, suggest that the backbone formed by the IFT-B complex does not completely disassemble at the tip. Such a possibility has been proposed also by Wingfield et al. (2021) on the basis of in vivo studies on *Chlamydomonas* IFT dynamics. These authors found that the anterograde trains do not undergo a complete disassembly, rather they either fragment into shorter segments or convert directly into retrograde trains. In these studies, IFT-A and IFT-B showed similar turnaround kinetics, possibly suggesting that the two complexes remain associated during train remodelling. Using a different approach, we have been unable to localise IFT-A proteins still associated to IFT-B at the tip. It is possible that, though turning around with a similar kinetics, IFT-A dissociates at the tip from IFT-B or, alternatively, that it dissociates under our experimental conditions. Hence, further studies are required to address this point.

AUTHOR CONTRIBUTIONS

Ambra Pratelli and Dalia Corbo performed most electron microscopy and immunolabelling experiments, Pietro Lupetti contributed to data discussion and manuscript writing, Caterina Mencarelli conceived and supervised the study, performed the tomogram segmentation and wrote the manuscript.

ACKNOWLEDGEMENTS

The authors wish to thank Eugenio Paccagnini and Mariangela Gentile for the acquisition of tomographic micrographs and post imaging tomogram reconstructions. Joel Rosenbaum (Yale University) and Cosima Tatiana Baldari are kindly acknowledged for critical reading of the manuscript. We thank Francesco Nardi for the statistical analysis reported in Figure 6b and David Mercati for technical assistance in plates preparation.

Open access funding provided by Universita degli Studi di Siena within the CRUI-CARE Agreement.

CONFLICT OF INTEREST

The authors declare no competing or financial interests.

ORCID

Caterina Mencarelli https://orcid.org/0000-0003-4530-8386

REFERENCES

Adams, G.M., Huang, B., Piperno, G. & Luck, D.J. (1981) Central-pair microtubular complex of *Chlamydomonas* flagella: polypeptide composition as revealed by analysis of mutants. *Journal of Cell Biology*, 91, 69–76. https://doi.org/10.1083/jcb.91.1.69

Al-Jassar, C., Andreeva, A., Barnabas, D.D., McLaughlin, S.H., Johnson, C.M., Yu, M. & van Breugel, M. (2017) The ciliopathy-associated Cep104 protein interacts with tubulin and Nek1 kinase. *Structure (London, England)*, 25, 146–156. https://doi.org/10.1016/j.str.2016.11.014

Braun, D.A. & Hildebrandt, F. (2017) Ciliopathies. *Cold Spring Harbor Perspectives in Biology*, 9, a028191. https://doi.org/10.1101/cshperspect.a028191

Brown, J.M., Cochran, D.A., Craige, B., Kubo, T. & Witman, G.B. (2015) Assembly of IFT trains at the ciliary base depends on IFT74. *Current Biology*, 25, 1583–93 https://doi.org/10.1016/j.cub.2015.04.060

Buey, R.M., Sen, I., Kortt, O., Mohan, R., Gfeller, D., Veprintsev, D., Kretzschmar, I., Scheuermann, J., Neri, D., Zoete, V., Michielin, O., María de Pereda, J., Akhmanova, A., Volkmer, R. & O Steinmetz, M. (2012) Sequence determinants of a microtubule tip localization signal (MtLS). *Journal of Biological Chemistry*, 287, 28227–28242. https://doi.org/10.1074/jbc.m112.373928

Buisson, J., Chenouard, N., Lagache, T., Blisnick, T., Olivo-Marin, J.C. & Bastin, P. (2013) Intraflagellar transport proteins cycle between the flagellum and its base. *Journal of Cell Science*, 126, 2059–2075. https://doi.org/10.1242/jcs.117069

Carbajal-González, B.I., Heuser, T., Fu, X., Lin, J., Smith, B.W., Mitchell, D.R. & Nicastro, D. (2013) Conserved structural motifs in the central pair complex of eukaryotic flagella. *Cytoskeleton*, 70, 101–120. https://doi.org/10.1002/cm.21094

Castellanos-Gonzalez, A., White, A.C., Ojo, K.K., Vidadala, R.S.R., Zhang, Z., Reid, M.C., Fox, A.M.W., Keyloun, K.R., Rivas, K. & Irani, A. (2013) A novel calcium- dependent protein kinase inhibitor as a lead compound for treating Cryptosporidiosis. *Journal of Infectious Diseases*, 208, 1342–1348. https://doi.org/10.1093/infdis/jit327

Chaya, T., Omori, Y., Kuwahara, R. & Furukawa, T. (2014) ICK is essential for cell type-specific ciliogenesis and the regulation of ciliary transport. *The EMBO Journal*, 33, 1227–1242. https://doi.org/10.1002/embj.201488175

Chien, A., Shih, S.M., Bower, R., Tritschler, D., Porter, M.E. & Yildiz, A. (2017) Dynamics of the IFT machinery at the ciliary tip. *ELife*, 6, e28606. https://doi.org/10.7554/elife.28606

Cole, D.G., Diener, D.R., Himelblau, A.L, Beech, P.L., Fuster, J.C. & Rosenbaum, J.L. (1998) *Chlamydomonas* kinesin-II–dependent Intraflagellar Transport (IFT): IFT particles contain proteins required

1768322x, 2022, 12, Downloaded from https://onlinelibrary.wiley.com/doi/10.1111/boc.202200038 by University Of Siena Sist Bibliot Di Ateneo, Wiley Online Library on [21/12/2022]. See the Terms and Conditions (https://onlinelibrary.wiley.com/terms-and-conditions) on Wiley Online Library for rules of use; OA articles are governed by the applicable Creative Commons License

for ciliary assembly in *Caenorhabditis elegans* sensory neurons. *Journal of Cell Biology*, 141, 993–1008. https://doi.org/10.1083/jcb.141.4.993

Craft Van de Weghe, J., Harris, J.A., Kubo, T., Witman, G.B. & Lechtreck, K.F. (2020) Diffusion rather than intraflagellar transport likely provides most of tubulin required for axonemal assembly in *Chlamydomonas*. *Journal of Cell Science*, 133, jcs249805. https://doi.org/10.1242/jcs.249805

Croft, J.T., Zabeo, D., Subramanian, R., & Höög, J.L. (2018) Composition, structure and function of the eukaryotic flagellum distal tip. *Essays in Biochemistry*, 62, 815–828. https://doi.org/10.1042/EBC20180032

Dentler, W.L. (1980) Structures linking the tips of ciliary and flagellar microtubules to the membrane. *Journal of Cell Science*, 42, 207–220.

Dentler, W.L. (2005) Intraflagellar transport (IFT) during assembly and disassembly of *Chlamydomona*s flagella. *Journal of Cell Biology*, 170, 649–659. https://doi.org/10.1002/yea.1284

Dentler, W.L. & Rosenbaum, J.L. (1977) Flagellar elongation and shortening in *Chlamydomonas*. III. structures attached to the tips of flagellar microtubules and their relationship to the directionality of flagellar microtubule assembly. *Journal of Cell Biology*, 74, 747–759. https://doi.org/10.1083/jcb.74.3.747

Dentler, W., Vanderwaal, K., & Porter, M.E. (2009) Recording and analyzing IFT in *Chlamydomonas* flagella. *Methods in Cell Biology*, 293, 145–55. https://doi.org/10.1016/S0091-679X(08)93008-9

Engel, B.D., Ludington, W.B. & Marshall, W.F. (2009) Intraflagellar transport particle size scales inversely with flagellar length: revisiting the balance-point length control model. *Journal of Cell Biology*, 187, 81–89. https://doi.org/10.1083/jcb.200812084

Frangakis, A. & Hegerl, R. (2001) Noise reduction in electron tomographic reconstruction using non linear anistropic diffusion. *Journal of Structural Biology*, 135, 239–250. https://doi.org/10.1006/jsbi.2001.4406

Geimer, S. (2009) Immunogold labeling of flagellar components in situ. *Methods in Cell Biology*, 91, 63–80. https://doi.org/10.1016/s0091-679x(08)91003-7

Gorman, D.S. & Levine, R.P. (1965) Cytochrome f and plastocyanin: their sequence in the photosynthetic electron transport chian of *Chlamydomonas reinhardtii*. *Proceedings of the National Academy of Sciences of the United States of America*, 54, 1665–1669. https://doi.org/10.1073/pnas.54.6.1665

Höög, J.L, Lacomble, S., O'Toole, E.T., Hoenger, A., McIntosh, J.R. & Gull, K. (2014) Modes of flagellar assembly in *Chlamydomonas reinhardtii* and *Trypanosoma brucei*. *eLIFE*, 3, e01479 https://doi.org/10.7554/elife.01479

Ichinose, S., Ogawa, T. & Hirokawa, N. (2015) Mechanism of Activity-Dependent Cargo Loading via the Phosphorylation of KIF3A by PKA and CaMKIIa. *Neuron*, 87, 1022–1035. https://doi.org/10.1016/j.neuron.2015.08.008

Johnson, K.A. & Rosenbaum, J.L. (1992) Polarity of flagellar assembly in Chlamydomonas. *Journal of Cell Biology*, 119, 1605–1611. https://doi.org/10.1083/jcb.119.6.1605

Jordan, M.A., Diener, D.R., Stepanek, L., & Pigino, G. (2018) The cryo-EM structure of intraflagellar transport trains reveals how dynein is inactivated to ensure unidirectional anterograde movement in cilia. *Nature Cell Biology*, 20, 1250–1255. https://doi.org/10.1038/s41556-018-0213-1

Kanie, T., Abbott, K.L., Mooney, N.A., Plowey, E.D., Demeter, J. & Jackson, P.K. (2017) The CEP19-RABL2 GTPase Complex Binds IFT-B to Initiate Intraflagellar Transport at the Ciliary Base. *Developmental Cell*, 42: 22–36. https://doi.org/10.1016/j.devcel.2017.05.016

Kozminski, K.G., Beech, P.L. & Rosenbaum, J.L. (1995) The *Chlamydomonas* kinesin- like protein FLA10 is involved in motility associated with the flagellar membrane. *Journal of Cell Biology*, 131, 1517–1527. https://doi.org/10.1083/jcb.131.6.1517

Kremer, J.R., Mastronarde, D.N. & McIntosh, J.R. (1996) Computer visualization of three-dimensional image data using IMOD. *Journal of Structural Biology*, 116, 71–76. https://doi.org/10.1006/jsbi.1996.0013

Lechtreck, K.-F., Gould, T.J. & Witman, G.B. (2013) Flagellar central pair assembly in *Chlamydomonas reinhardtii*. *Cilia*, 2, 15. https://doi.org/10.1186/2046-2530-2-15

Liang, Y., Pang, Y., Wu, Q., Hu, Z., Han, X., Xu, Y., Deng, H. & Pan, J. (2014) FLA8/KIF3B phosphorylation regulates kinesin-II interaction with IFT-B to control IFT entry and turnaround. *Developmental Cell*, 30, 585–597. https://doi.org/10.1016/j.devcel.2014.07.019

Ludington, W.B., Wemmer, K.A, Lechtreck, K.F., Witman, G.B. & Marshall, W.F. (2013) Avalanche-like behavior in ciliary import. *Proceedings of the National Academy of Sciences of the United States of America*, 110, 3925–3930. https://doi.org/10.1073/pnas.1217354110

Lucker, B.F., Behal, R.H., Qin, H., Siron, L.C., Taggart, W.D., Rosenbaum, J.L. & Cole, D.G. (2005) Characterization of the intraflagellar transport complex B core: Direct interaction of the IFT81 and IFT74/72 subunits. *Journal of Biological Chemistry*, 280, 27688–27696. https://doi.org/10.1074/jbc.m505062200

Marshall, W.F. & Rosenbaum, J.L. (2001) Intraflagellar transport balances continuous turnover of outer doublet microtubules: implications for flagellar length control. *Journal of Cell Biology*, 155, 405–14. https://doi.org/10.1083/jcb.200106141.

Mencarelli, C., Mitchell, A., Leoncini, R., Rosenbaum, J. & Lupetti, P. (2013) Isolation of intraflagellar transport trains. *Cytoskeleton*, 70, 439–452. https://doi.org/10.1002/cm.21121

Mijalkovic, J., Prevo, B., Oswald, F., Mangeol, P. & Peterman, E.J.G. (2017) Ensemble and single-molecule dynamics of IFT dynein in *Caenorhabditis elegans* cilia. *Nature Communication*, 8, 14591. https://doi.org/10.1038/ncomms14591

Nakayama, K. & Katoh, Y. (2020) Architecture of the IFT ciliary trafficking machinery and interplay between its components. *Critical Reviews in Biochemistry and Molecular Biology*, 55, 179–196. https://doi.org/10.1080/10409238.2020.1768206

Nievergelt, A.P., Zykov, I., Diener, D., Chhatre, A., Buchholz, T.-.O., Delling, M., Diez, S., Jug, F., Stěpánek, L. & Pigino, G. (2022) Conversion of anterograde into retrograde trains is an intrinsic property of intraflagellar transport. *Current Biology*, 32, 1–8. https://doi.org/10.1016/j.cub.2022.07.033

Nishijima, Y., Hagiya, Y., Kubo, T., Takei, R., Katoh, Y. & Nakayama, K. (2017) RABL2 interacts with the intraflagellar transport-B complex and CEP19 and participates in ciliary assembly. *Molecular Biology of the Cell*, 28, 1652–1666. https://doi.org/10.1091/mbc.e17-01-0017

Oh, Y.S., Wang, E.J., Gailey, C.D., Brautigan, D.L., Allen, B.L. & Fu, Z. (2019) Ciliopathy-associated protein kinase ICK requires its non-catalytic carboxyl-terminal domain for regulation of ciliogenesis. *Cells*, 8, 677. https://doi.org/10.3390/cells8070677

Pazour, G.J., Dickert, B.L. & Witman, G.B. (1999) The DHC1b (DHC2) isoform of cytoplasmic dynein is required for flagellar assembly. *Journal of Cell Biology*, 144, 473–481. https://doi.org/10.1083/jcb.144.3.473

Pedersen, L.B., Miller, M.S., Geimer, S., Leitch, J.M., Rosenbaum, J.L. & Cole, D.G. (2005) *Chlamydomonas* IFT172 is encoded by FLA11, interacts with CrEB1, and regulates IFT at the flagellar tip. *Current Biology*, 15, 262–266. https://doi.org/10.1016/j.cub.2005.01.037

Pedersen, L.B., Geimer, S. & Rosenbaum, J.L. (2006) Dissecting the molecular mechanisms of intraflagellar transport in *Chlamydomonas*. *Current Biology*, 16, 450–459. https://doi.org/10.1016/j.cub.2006.02.020

Pettersen, E.F., Goddard, T.D., Huang, C.C., Couch, G.S., Greenblatt, D.M., Meng, E. & Ferrin, T.E. (2004) UCSF Chimera. A visualization system for exploratory research and analysis. *Journal of Computational Chemistry*, 25, 1605–1612. https://doi.org/10.1002/jcc.20084

1768322x, 2022, 12, Downloaded from https://onlinelibrary.wiley.com/doi/10.1111/boc.202200038 by University Of Siena Sist Bibliot Di Ateneo, Wiley Online Library on [21/12/2022]. See the Terms and Conditions (https://onlinelibrary.wiley.com/terms-and-conditions) on Wiley Online Library for rules of use; OA articles are governed by the applicable Creative Commons License

Pigino, G., Geimer, S., Lanzavecchia, S., Paccagnini, E., Cantele, F., Diener, D.R., Rosenbaum, J.L & Lupetti, P. (2009) Electron-tomographic analysis of intraflagellar transport particle trains in situ. *Journal of Cell Biology*, 187, 135–148. https://doi.org/10.1083/jcb.200905103

Piperno, G. & Mead, K. (1997) Transport of a novel complex in the cytoplasmic matrix of *Chlamydomonas* flagella. *Proceedings of the National Academy of Sciences of the United States of America*, 94, 4457–4462. https://doi.org/10.1073/pnas.94.9.4457

Porter, M.E., Bower, R., Knott, J.A., Byrd, P. & Dentler, W. (1999) Cytoplasmic dynein heavy chain 1b is required for flagellar assembly in *Chlamydomonas*. *Molecular Biology of the Cell*, 10, 693–712. https://doi.org/10.1091/mbc.10.3.693

Qin, H., Wang, Z., Diener, D. & Rosenbaum, J. (2007) Intraflagellar transport protein 27 is a small G protein involved in cell-cycle control. *Current Biology*, 17, 193–202. https://doi.org/10.1016/j.cub.2006.12.040

R Core Team (2021) *R: A language and environment for statistical computing*. R Foundation for Statistical Computing. http://www.R-project.org

Reiter, J.F. & Leroux, M.R. (2017) Genes and molecular pathways underpinning ciliopathies. *Nature Reviews Molecular Cell Biology*, 18, 533–547. https://doi.org/10.1038/nrm.2017.60

Ringo, D.L. (1967) Flagella motion and fine structure of the flagellar apparatus in *Chlamydomonas*. *Journal of Cell Biology*, 33, 543–571. https://doi.org/10.1083/jcb.33.3.543

Reynolds, E.S. (1963) The use of lead citrate at high pH as an electron-opaque stain in electron microscopy. *Journal of Cell Biology*, 17, 208–212. https://doi.org/10.1083/jcb.17.1.208

Reynolds, M.J., Phetruen, T., Fisher, R.L., Chen, K., Pentecost, B.T., Gomez, G., Ounjai, P. & Sui, H. (2018) The developmental process of the growing motile ciliary tip region. *Science Reports*, 8, 7977. https://doi.org/10.1038/s41598-018-26111-2

Rosenbaum, J.L. & Child, F.M. (1967) Flagellar regeneration in protozoan flagellates. *Journal of Cell Biology*, 34, 345–64. https://doi.org/10.1083/jcb.34.1.345

Satish-Tammana, T.V., Tammana, D., Diener, D.R. & Rosenbaum, J.L. (2013) Centrosomal protein CEP104 (*Chlamydomonas* FAP256) moves to the ciliary tip during ciliary assembly. *Journal of Cell Science*, 126, 5018–5029. https://doi.org/10.1242/jcs.133439

Soares, H., Carmona, B., Nolasco, S., Viseu Melo, L. & Gonçalves, J. (2019) Cilia distal domain: diversity in evolutionarily conserved structures. *Cells*, 8, 160. https://doi.org/10.3390/cells8020160

Stepanek, L. & Pigino, G. (2016) Microtubule doublets are double-track railways for intraflagellar transport trains. *Science*, 352, 721–724. https://doi.org/10.1126/science.aaf4594

Taschner, M. & Lorentzen, E. (2016) The intraflagellar transport machinery. *Cold Spring Harbor Perspectives in Biology*, 8, a028092. https://doi.org/10.1101/cshperspect.a028092

Teves, M.E., Nagarkatti-Gude, D.R., Zhang, Z. & Strauss, J.F. (2016) Mammalian axoneme central pair complex proteins: broader roles revealed by gene knockout phenotypes. *Cytoskeleton*, 73, 3–22. https://doi.org/10.1002/cm.21271

Tsao, C.C. & Gorovsky, M.A. (2008) Different effects of Tetrahymena IFT172 domains on anterograde and retrograde intraflagellar transport. *Molecular Biology of the Cell*, 19, 1450–1461. https://doi.org/10.1091/mbc.e07-05-0403

Vannuccini, E., Paccagnini, E., Cantele, F., Gentile, M., Dini, D., Fino, F., Diener, D., Mencarelli, C. & Lupetti, P. (2016) Two classes of short IFT trains with different 3D structure are present in *Chlamydomonas* flagella. *Journal of Cell Science*, 129, 2064–74. https://doi.org/10.1242/jcs.183244

Wang, Q., Taschner, M., Ganzinger, K.A., Kelley, C., Villasenor, A., Heymann, M., Schwille, P., Lorentzen, E. & Mizuno, N. (2018) Membrane association and remodeling by intraflagellar transport protein IFT172. *Nature Communication*, 9, 4684. https://doi.org/10.1038/s41467-018-07037-9

Wickham, H. (2016) *ggplot2: elegant graphics for data analysis*. Springer-Verlag, ISBN 978-3-319-24277-4, http://ggplot2.tidyverse.org.

Wingfield, J.L., Mekonnen, B., Mengoni, I., Liu, P., Jordan, M., Diener, D., Pigino, G. & Lechtreck, K. (2021) In vivo imaging shows continued association of several ITF-A, B and dynein complexes while IFT trains U-turn at the tip. *Journal of Cell Science*, 134, jcs.259010. https://doi.org/10.1242/jcs.259010.

SUPPORTING INFORMATION

Additional supporting information can be found online in the Supporting Information section at the end of this article.

How to cite this article: Pratelli, A., Corbo, D., Lupetti, P. & Mencarelli, C. (2022) The distal central pair segment is structurally specialised and contributes to IFT turnaround and assembly of the tip capping structures in *Chlamydomonas* flagella. *Biology of the Cell*, 114, 349–364. https://doi.org/10.1111/boc.202200038

1768322x, 2022, 12, Downloaded from https://onlinelibrary.wiley.com/doi/10.1111/boc.202200038 by University Of Siena Sist Bibliot Di Ateneo, Wiley Online Library on [21/12/2022]. See the Terms and Conditions (https://onlinelibrary.wiley.com/terms-and-conditions) on Wiley Online Library for rules of use; OA articles are governed by the applicable Creative Commons License